CHROMATICITY COMPENSATION OF A GHOST COLLIDER*

B. R. Gamage†, A. Hutton, Jefferson Lab, Newport News, VA, USA
Peter Williams, STFC Daresbury Laboratory / Cockcroft Institute, Daresbury, UK

Abstract

The GHOST collider final focus system is a pure quadrupole-drift beamline targeting $\beta^* = 2$ mm at four serial interaction points, with peak β-functions reaching ~65 km in the final triplet. Beam tracking simulations reveal that a nominal bunch develops a pronounced C-shape in longitudinal phase space at IP1, with σ_z growing from 0.15 mm to ~2.3 mm — a factor of ~15× increase that directly reduces luminosity. The mechanism is identified as *chromatically amplified betatron path length*: off-momentum particles acquire enlarged betatron amplitudes in the high-β final triplet, generating excess path length via the geometric $\Delta z = -\frac{1}{2}\int (x'^2 + y'^2)\, ds$ integral. Within the monoenergetic Balandin framework, $\epsilon^2\xi^2$ with $\xi = -\frac{1}{2}\int \gamma\, ds$ dominates $\epsilon^2 W^2$ by over four million times; the full beam σ_z is a further factor of ~27 larger, driven by σ_δ-induced chromatic amplitude growth. Phase-advance scans confirm that σ_z is insensitive to the apochromatic ($W \approx 0$) condition. When combined with the geometric hourglass effect, this distortion poses a challenge to maximizing luminosity within the current lattice design.

INTRODUCTION

The GHOST collider [1, 2] final-focus system is a pure quadrupole-drift beamline designed to achieve $\beta^* = 2$ mm at four serial interaction points (IPs) without the use of dipole magnets. The absence of dipoles eliminates synchrotron radiation in the final focus — a significant advantage at high beam energy — but also removes dispersion, precluding conventional sextupole-based chromatic correction. Instead, chromatic correction is performed via phase advance tuning through a matching section, minimizing the Montague W-function [3] at each IP to make them apochromatic [4]. The extreme demagnification required to achieve $\beta^* = 2$ mm produces peak β-functions of order 65 km in the final triplet quadrupoles immediately upstream of each IP.

During beam tracking studies of IP1, a striking C-shaped distortion was observed in the longitudinal phase space: a bunch initialized with nominal parameters develops a non-Gaussian distribution by the time it reaches the IP, with the bunch length growing by a factor of ~15. With $\sigma_z \approx 2.3$ mm comparable to $\beta^* = 2$ mm, this has direct implications for luminosity through bunch lengthening, a non-Gaussian profile, and a significant geometric hourglass effect even when beam-beam effects are neglected.

This paper identifies the mechanism driving the C-shape, quantifies it using the Balandin framework [5], and demonstrates that it is governed by a quantity distinct from the W-function. The nominal beam parameters are given in Table 1.

Table 1: Nominal GHOST Beam Parameters at IP1

Parameter	Symbol	Value
Beam energy	E	275 GeV
Geometric emittance	$\epsilon_{x,y}$	4×10^{-9} m rad
RMS energy spread	σ_δ	2.9×10^{-4}
Initial bunch length	σ_z	0.15 mm
IP beta function	β^*	2 mm
Peak beta in final triplet	$\beta_{\max}$	~65,000 m
Hourglass parameter	σ_z/β^*	~1.15

THE GHOST LATTICE

The lattice consists of four symmetric half-IP sections repeated serially, each de-magnifying from a starting waist down to $\beta^* = 2$ mm at the IP through an upstream and downstream final-focus triplet. The matching section between cells provides sufficient degrees of freedom to control the phase advance independently in both transverse planes. This is used to set $W_a \approx 10$, $W_b \approx 6$ at IP1 in closed geometry — nearly apochromatic — through destructive interference of the ~25,000 peaks of W generated in the upstream and downstream triplets. Figure 1 shows β and W along the beamline to IP1.

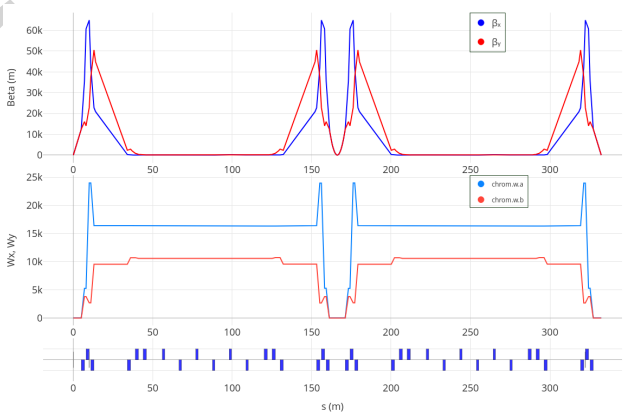

Figure 1: β_x, β_y (top) and Montague W-function (bottom) along the GHOST beamline to IP1. Peak $\beta \approx 65$ km in the final triplet. $W \approx 10$ at IP1 (dotted line) confirms near-apochromatic conditions.

* Work supported by Jefferson Science Associates, LLC under U.S. DOE Contract DE-AC05-06OR23177
† randika@jlab.org

LONGITUDINAL PHASE SPACE DISTORTION

Observation

Phase space at IP1 for the nominal beam, with each particle colored by its momentum offset p_z is shown in Fig. 2. The longitudinal (z, p_z) panel reveals the characteristic C-shape: the on-momentum core ($p_z \approx 0$, yellow-green) arrives at $z \approx 0$, while the energy tails (red: $\delta > 0$, blue: $\delta < 0$) are displaced to large negative z, indicating late arrival in tails. The transverse panels reveal that these same off-momentum particles — which arrive late — also carry the largest transverse amplitudes, with σ_x reaching hundreds to thousands of µm for the energy tails compared to ∼3 µm for the on-momentum core. This direct coupling between longitudinal and transverse phase space distortion is the hallmark of the chromatic betatron path length mechanism.

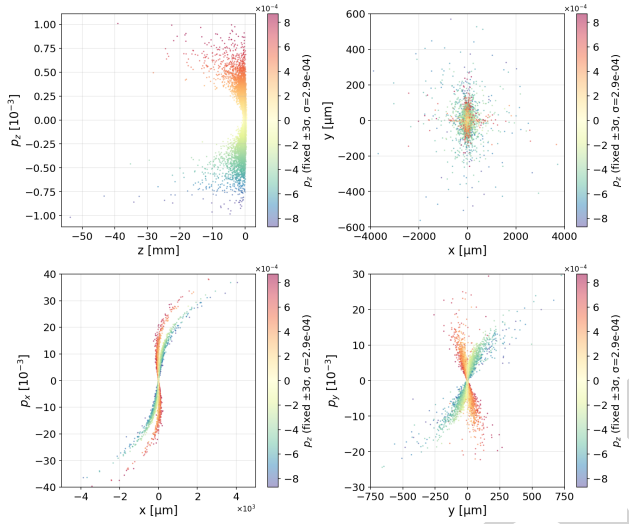

Figure 2: Phase space at IP1 colored by p_z (blue: $\delta < 0$, yellow-green: $\delta \approx 0$, red: $\delta > 0$). Longitudinal (z, p_z): C-shape with both energy tails ($\delta > 0$ and $\delta < 0$) displaced symmetrically to large negative z, confirming the path length delay scales as $|\delta|$ regardless of sign — a second-order chromatic effect. Transverse (x, y), (x, p_x), (y, p_y): the same off-momentum particles carry the largest transverse amplitudes, directly showing the coupling between longitudinal and transverse distortion.

Mechanism

The physical origin is the geometric path-length integral, exact for any drift-quadrupole system with no dipoles ($h = 0$) [6]:

$$\Delta z = -\frac{1}{2}\int_0^L \left[x'(s)^2 + y'(s)^2\right] ds. \qquad (1)$$

The integral has no explicit δ dependence; the momentum offset enters via chromatic focusing errors $\Delta k = -k\delta$ that perturb the betatron amplitude of off-momentum particles. In the high-β final triplet, even small chromatic errors produce large amplitude perturbations, accumulating extra path length via Eq. (1). Since this perturbation scales as $|\delta|$, both energy tails arrive late while the on-momentum core arrives on time, producing the C-shape. The delay depends quadratically on δ — a second-order chromatic effect, not a first-order dispersive one.

Separating Effects

Three controlled tracking cases with $\sigma_z(0) = 0\sigma_z(0) = 0\sigma_z(0) = 0$ isolate the contributing mechanisms:

1. **Transverse emittance only** ($\epsilon_{x,y} = 4$ nm, $\sigma_\delta = 0$): pure geometric betatron path length gives $\sigma_z = 86$ µm via Eq. (1).

2. **Energy spread only** ($\epsilon_{x,y} \to 0$, $\sigma_\delta = 2.9 \times 10^{-4}$): gives $\sigma_z \approx 0$. With $\eta = 0$, particles stay on the reference orbit and Eq. (1) vanishes. This rules out R_{56} and direct longitudinal map terms.

3. **Nominal beam** ($\epsilon_{x,y} = 4$ nm, $\sigma_\delta = 2.9 \times 10^{-4}$): gives $\sigma_z = 2.197$ mm, a factor of 27.2× larger than case (1).

The 27× amplification confirms that the effect requires both transverse emittance and energy spread simultaneously — neither alone produces significant bunch lengthening.

QUANTIFICATION: BALANDIN FRAMEWORK

For a monoenergetic Gaussian beam, Balandin et al. [5] derived the bunch length variance growth from betatron oscillations alone:

$$\sigma_z^2(L) = \sigma_z^2(0) + \epsilon_x^2\left(\xi_x^2 + \zeta_x^2 + \eta_x^2\right) + \epsilon_y^2\left(\xi_y^2 + \zeta_y^2 + \eta_y^2\right), \quad (2)$$

where $\xi_{x,y} = -\frac{1}{2}\int_0^L \gamma_{x,y}\, ds$ are the Balandin chromaticities and $\zeta_{x,y}$, $\eta_{x,y}$ are the apochromaticities related to the W-function. As shown in Fig. 3, γ peaks in the regions of large α immediately upstream and downstream of the β maxima, and ξ accumulates predominantly across the two final-triplet regions. Crucially, since $\gamma > 0$ everywhere, the ξ integral is monotonically accumulating: there is no phase-advance condition that can cancel it, in contrast to the W-function whose chromatic Twiss derivatives oscillate and can be made to interfere destructively at the IP.

The chromaticities are computed from Bmad/Tao Twiss data [7]: $\xi_x \approx -21{,}406$, $\xi_y \approx -12{,}906$ (both dimensionless) at the nominal operating point. Table 2 compares the $\epsilon^2\xi^2$ and $\epsilon^2 W^2$ contributions at the nominal (apochromatic) operating point in closed geometry.

Table 2: Contributions to the Monoenergetic Balandin Variance, Eq. (2), at the Nominal (Apochromatic) Operating Point ($W_a = 10.2$, $W_b = 6.4$, Closed Geometry)

Quantity	Value	
$\epsilon^2\xi^2$ (both planes)	$\sim 1 \times 10^{-8}$ m^2	dominant
$\epsilon^2 W^2$ (both planes)	$\sim 2 \times 10^{-15}$ m^2	negligible
Ratio	$\sim 4.3 \times 10^6$	

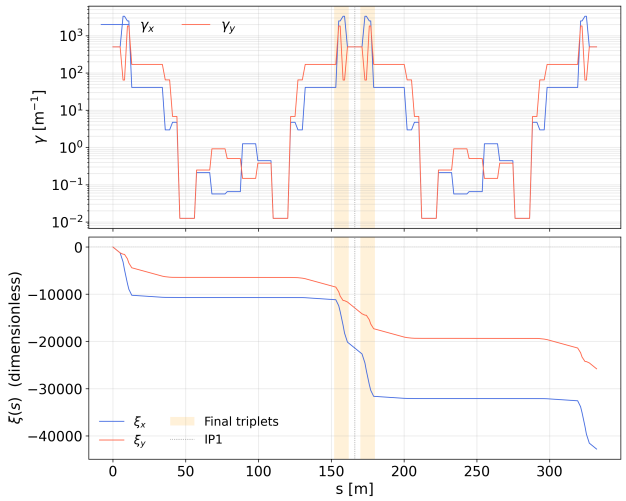

Figure 3: Top: Twiss $\gamma_{x,y}$ along the GHOST beamline (log scale), the integrand of the Balandin chromaticity. Bottom: cumulative $\xi(s) = -\frac{1}{2}\int_0^s \gamma\, ds$ for both planes. The final triplet regions (orange) dominate the accumulation. Because $\gamma > 0$ everywhere, ξ accumulates monotonically and is unaffected by the apochromatic cancellation of W at IP1 (dotted).

The ξ term dominates by over four million times. Substituting the GHOST values into Eq. (2) gives $\sigma_z \approx 100\,\mu$m, in agreement with the Case (1) tracking result of 86 µm. The Case (3) full-beam result of 2.197 mm is a factor of ~27 larger; this excess is the σ_δ-driven chromatic-amplitude contribution described qualitatively above, in which off-momentum particles acquire enlarged betatron amplitudes in the high-β triplet that feed into Eq. (1).

To verify the W-insensitivity near the current nominal value empirically, phase-advance scans were performed by varying the matching quadrupoles to scan W_a and W_b at IP1 independently while tracking the nominal beam. Both planes were constrained simultaneously — when scanning W_a, the μ_y phase advance was held fixed at its nominal value, and vice versa. Figure 4 shows that despite W_a varying by a factor of ~8 across the scan, σ_z changes by less than 1.3 %.

This confirms the prediction of Fig. 3: the apochromatic condition ($W \approx 0$) ensures off-momentum particles are focused to the correct β^* at IP1, but does not constrain the path length accumulated en route, which is governed by the monotonically-accumulating ξ.

LUMINOSITY IMPACT

The longitudinal distortion degrades luminosity through three channels. The ~15× increase in σ_z directly reduces peak luminosity ($\mathcal{L} \propto 1/\sigma_z$). The non-Gaussian C-shape further reduces the luminosity integral via the convolution of the two bunch profiles. Finally, with $\sigma_z/\beta^* \approx 1.15$, the geometric hourglass effect — purely geometric for GHOST neutral bunches, with particles at longitudinal position z encountering $\beta(z) = \beta^* + z^2/\beta^*$.

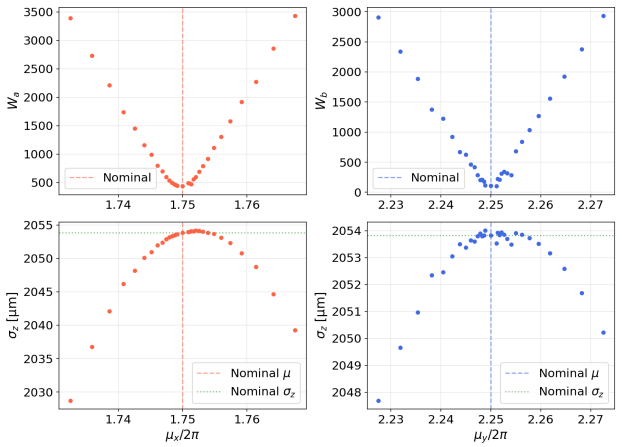

Figure 4: σ_z at IP1 vs. W_a (left) and W_b (right). W_a and W_b vary by factors of ~8 and ~30 respectively, while σ_z changes by ≤ 1.3 %. This confirms σ_z is relatively insensitive to the apochromatic condition in both planes.

The combined effect cannot be recovered through apochromatic phase tuning alone, since σ_z is set by the integrated chromatic dynamics in the triplet rather than by the IP focusing condition.

CONCLUSION

Beam tracking reveals severe longitudinal and transverse phase space distortion in the GHOST IP1 final focus, driven by chromatically-amplified betatron path length in the high-β final triplet. Within the monoenergetic Balandin framework, $\epsilon^2\xi^2$ exceeds $\epsilon^2 W^2$ by $\sim 4.3 \times 10^6$ and reproduces the Case (1) result; the full-beam σ_z is ~27× larger, driven by σ_δ-induced chromatic amplitude growth. Phase-advance scans confirm σ_z is insensitive to W across a factor of ~73: the apochromatic condition governs transverse focusing at the IP, not integrated chromatic dynamics. The resulting bunch lengthening, non-Gaussian profile, and geometric hourglass ($\sigma_z/\beta^* \approx 1.15$) together may represent a fundamental limitation unless additional correction mechanisms, such as controlled dispersion and sextupoles, are introduced.

We are planing to introduce controlled dispersion oscillations that cross each IP with $\eta = 0$ but $\eta' \neq 0$, preserving the dispersion free condition at the IP while creating dispersive regions upstream where sextupoles can be placed [8]. Since sextupoles provide δ^2-order chromatic correction — the same order as the C-shape path length smearing — they are the natural corrector for this effect. The phase advance separation between the four serial IPs can be exploited to realize a global correction scheme. We are developing this scheme and will report on it in the future.

ACKNOWLEDGEMENT

The authors would like to thank Rogelio Tomás García for the valuable insights provided into this work.

REFERENCES

[1] A. Hutton, R. Apsimon, B. Gamage, M. Joshi, P. Williams, and K. Yokoya, "The Ghost Collider: an innovative Higgs Factory", presented at the IPAC'26, Deauville, France, May 2026, paper MOO1T02, this conference.

[2] P. Williams, R. Apsimon, B. Gamage, A. Hutton, M. Joshi, and K. Yokoya, "The Linear Ghost Collider: an efficient Higgs Factory", presented at the IPAC'26, Deauville, France, May 2026, paper MOP1022, this conference.

[3] B. W. Montague, "Linear optics for improved chromaticity correction", CERN, Geneva, Switzerland, Rep. CERN-LEP-Note-165, 1979. https://cds.cern.ch/record/67243

[4] C. A. Lindstrøm and E. Adli, "Design of general apochromatic drift-quadrupole beam lines", *Phys. Rev. Accel. Beams*, vol. 19, p. 071002, Jul. 2016. doi:10.1103/PhysRevAccelBeams.19.071002

[5] V. Balandin, R. Brinkmann, W. Decking, and N. Golubeva, "Apochromatic Beam Transport in Drift-Quadrupole Systems", in *Proc. IPAC'10*, Kyoto, Japan, May 2010, paper THPD083, pp. 4476–4478.

[6] Y. Shoji, "Dependence of average path length on betatron motion in a storage ring", *Phys. Rev. Spec. Top. Accel. Beams*, vol. 8, p. 094001, Sep. 2005. doi:10.1103/PhysRevSTAB.8.094001

[7] D. Sagan, "Bmad: A relativistic charged particle simulation library", *Nucl. Instrum. Methods Phys. Res. A*, vol. 558, pp. 356–359, Mar. 2006. doi:10.1016/j.nima.2005.11.001

[8] P. Raimondi and A. Seryi, "Novel final focus design for future linear colliders", *Phys. Rev. Lett.*, vol. 86, p. 3779, Apr. 2001. doi:10.1103/PhysRevLett.86.3779